Real-Time Voltage-Stability Enhancement via Demand Response

Mohammadhafez Bazrafshan
Dept. Civil & Environ. Eng.
University of Colorado Boulder
Boulder, CO
hafez.bazrafshan@icloud.com

Hao Zhu
Dept. Electrical & Computer Eng.
The University of Texas at Austin
Austin, TX
haozhu@utexas.edu

Nikolaos Gatsis
Dept. Electrical & Computer Eng.
The University of Texas at San Antonio
San Antonio, TX
nikolaos.gatsis@utsa.edu

***Abstract*—We propose a real-time algorithm that improves the voltage stability of a power network by rearranging the consumption level of loads participating in demand response (DR). Towards this end, we revisit an optimization problem that seeks to maximize the smallest singular value (SSV) of the power flow Jacobian subject to nonconvex power flows and limit constraints on voltages of PQ buses, real power generation of the slack generator, and reactive power generation of the slack and PV buses. Instead of linearizations or relaxations, we penalize the limit constraints and rely on network measurements to derive an online projected gradient update to determine DR decisions. The updated DR decisions are applied to the power network per iteration and latest measurements are fed back to the algorithm. Simulations on several standard transmission networks demonstrate that the proposed methodology improves the value of the SSV of the power flow Jacobian per time step while avoiding significant bound violations.**

***Index Terms*—Voltage stability, smallest singular value, demand response, feedback-based optimization**

I. Introduction

After a major disturbance, such as loss of a transmission line or a generation unit, power system loads attempt to restore power consumption to their pre-disturbance values. If the disturbance is not remedied, such a process potentially calls for power transfers beyond the transmission capability of the network and its generator units. At this stage, uncontrollable voltage drops evince at various ends of the network. This phenomenon is referred to as *voltage instability*, and if not prevented, may result in a network-wide voltage collapse [1]. For instance, voltage instability appears to have been the primary technical cause of the 2003 North American blackout [2].

In order to detect and prevent voltage instability, various *voltage-stability indices* (VSIs) have been proposed, which, in one way or another, compute a notion of distance between the power grid operating point and a point at which voltage collapses [3]. A popular choice are VSIs based on the computation of maximum power transfer limits [4], [5]. Given an initial operating point, these indices are obtained by tracing the power flow solution through continuation power flow, by e.g., scaling of loads or generations [6].

An equally popular choice are VSIs that measure the distance to singularity of the power flow Jacobian [7]. Such indices encompass arbitrary changes in loads or generations and rely on the observation that during a voltage collapse, the Jacobian becomes singular. In this group, the smallest singular value (SSV) of the power flow Jacobian stands out [8].

Of course, efficient computation of the SSV remains a practical challenge [9]. Recently, more computationally tractable Jacobian-based VSIs have been considered. For example, the work of [10], for a VSI based on a sufficiency condition on the Jacobian nonsingularity that appears as a conic inequality for constant loads, or the VSI proposed in [11] that affords a completely distributed computation in distribution networks.

Depending on the application, a carefully-selected VSI may enter an optimal power flow (OPF) problem as an objective so that a maximum distance to voltage collapse is ensured, for example, [12] and [13, Eq. (10)], or as a constraint, so that the optimal steady-state operating point is ensured to be a threshold distance from voltage collapse [10], [14], [15]. These works ultimately rely on actions of generators, capacitors, and synchronous condensers to deliver their purpose. Load-shedding may also be viable as a last resort [16].

Generator response time to disturbances are restricted by ramp constraints. Therefore, recent research has looked at demand response for voltage stability improvement, based on the premise that flexible loads can react more quickly [17]–[19]. While the total power consumption remains constant to maintain system frequency, a different loading pattern can be immediately coordinated that is more favorable for voltage stability. Based on AC power flow linearizations and computation of SSV sensitivities, an iterative linear programming algorithm is designed in [17]–[19], to this end.

In this paper, we consider a similar problem. Specifically, we consider maximizing the SSV of the power flow Jacobian subject to bound constraints on network voltages, real and reactive power generation, as well as the nonconvex power flow equations. The constant total-demand constraint of demand-responsive loads are also included. Our solution methodology, nevertheless, is markedly different from [17]–[19]. Instead of

This material is based upon work supported by the National Science Foundation under Grant No. ECCS-1610732 and ECCS-1653706, and ECCS-1847125.

978-1-7281-0407-2/19/$31.00

power flow linearizations, we exploit the formulation to derive an online gradient projection scheme to approximately solve the original nonconvex problem. The proposed algorithm relies on measurements to calculate the required updates, but it is applied *per-iteration* to the power network and manages to improve the SSV in real time.

There has recently been a surging interest in feedback-based optimization methods for OPF that all leverage network measurements to calculate real-time control commands that must be exerted back on to the network. The basis for algorithm design in these methodologies seem to fall in three distinct categories. The first category relies on the grid as an *implicit power flow solver* [20]–[22], while using a model-based gradient calculation via the implicit function theorem to update controller setpoints. The second category [23]–[26] leverages a linearized form of power flow equations—valid for distribution networks—to derive real-time controller updates. The design usually incorporates network measurements in place of uncontrollable variables per iteration. Finally, a third category applies the projected gradient-descent to a constrained optimization problem on the power flow manifold [27], [28]. The controller updates obtained are then applied to the nonlinear physical network. While we acknowledge that there might be theoretical connections between the three categories of feedback-based optimization methods for OPF, we do not explore this here. We highlight, however, that our construction coalesces with the first category [20]–[22]. The projection step, however, is modified to handle the constant total-demand constraint of demand response.

The organization of this manuscript is as follows. Section II describes the network model, lays out the objective and constraints of an optimization for voltage-stability enhancement via demand response. Section III develops reformulates the problem and proposes a gradient projection algorithm to solve it in real-time. Numerical experiments on three standard power networks are carried out in Section IV.

Notation: For a set $\mathcal{A}$ (denoted by the Caligraphic typeset of A), its cardinality is denoted by the italic capital A. Column vectors are denoted by lower-case letters. For vector x, index set $\mathcal{A}$, and an index $i \in \mathcal{A}$, denote respectively by x_i and $x_{\mathcal{A}}$, the element of x corresponding to the index i and a vector of size A comprised of x_i's for all $i \in \mathcal{A}$. For a vector x, $[x]$ denotes a diagonal matrix with x on the diagonal. For a matrix X, X' and $\lambda_0(X)$ denote its transpose and smallest eigenvalue, respectively.

II. Network model and description of the problem

A power transmission network is mathematically modeled by an undirected, connected graph, denoted here by the two-tuple $(\mathcal{N}, \mathcal{E})$ where $\mathcal{N}$ is the set of nodes (buses) and $\mathcal{E} \subseteq \mathcal{N} \times \mathcal{N}$ is the set of edges (transmission lines and transformers). It is typical to partition the set of nodes as $\mathcal{N} = \mathcal{Q} \cup \mathcal{V} \cup \{s\}$ where the sets $\mathcal{Q}$ and $\mathcal{V}$ respectively collect PQ and PV buses while s denotes the index of the slack bus. Furthermore, we suppose that a set $\mathcal{D} \subseteq \mathcal{N} \setminus \{s\}$ collects buses that participate in demand response.

Let θ, v, p, and q respectively denote the vector of voltage angles, voltage magnitudes, net real power injections, and net reactive power injections, collected for all buses in $\mathcal{N}$. Let $G+jB$ be the complex network admittance matrix. It is convenient to define the following power balance functions:

$$\begin{aligned}\mathfrak{p}(\theta, v, p) &:= [v][\cos\theta]G[v]\cos\theta + [v][\sin\theta]B[v]\cos\theta \\ &\quad + [v][\sin\theta]G[v]\sin\theta - [v]\cos\theta B[v]\sin\theta - p \qquad (1a)\\ \mathfrak{q}(\theta, v, q) &:= [v][\sin\theta]G[v]\cos\theta - [v]\cos\theta B[v]\cos\theta \\ &\quad - [v]\cos\theta G[v]\cos\theta - [v][\sin\theta]B[v]\cos\theta - q. \qquad (1b)\end{aligned}$$

Let us further denote respectively by p_{g}, q_{g}, p_{d}, and q_{d} the vectors of real and reactive power generations and demands collected for all buses in $\mathcal{N}$. Then, the power flow equations are given by [6], [29]:

$$\mathfrak{p}(\theta, v, p_{\mathrm{g}} - p_{\mathrm{d}}) = 0 \qquad (2a)$$
$$\mathfrak{q}(\theta, v, q_{\mathrm{g}} - q_{\mathrm{d}}) = 0. \qquad (2b)$$

During a demand response operation, the power-flow operating point $y = (\theta, v, p_{\mathrm{g}}, q_{\mathrm{g}}, p_{\mathrm{d}}, q_{\mathrm{d}})$ must satisfy the following constraints:

$$\begin{aligned}
\theta_i &= \theta_s^{\mathrm{sp}} && i = s && (3a)\\
v_i &= v_i^{\mathrm{sp}} && i \in \mathcal{V} \cup \{s\} && (3b)\\
v_i^{\min} &\le v_i \le v_i^{\max} && i \in \mathcal{Q} && (3c)\\
p_{\mathrm{g}_i} &= p_{\mathrm{g}_i}^{\mathrm{sp}} && i \in \mathcal{Q} \cup \mathcal{V} && (3d)\\
p_{\mathrm{g}_s}^{\min} &\le p_{\mathrm{g}_i} \le p_{\mathrm{g}_s}^{\max} && i = s && (3e)\\
q_{\mathrm{g}_i} &= q_{\mathrm{g}_i}^{\mathrm{sp}} && i \in \mathcal{Q} && (3f)\\
q_{\mathrm{g}_i}^{\min} &\le q_{\mathrm{g}_i} \le q_{\mathrm{g}_i}^{\max} && i \in \mathcal{V} \cup \{\mathrm{s}\} && (3g)\\
p_{d_i} &= p_{d_i}^{\mathrm{sp}} && i \in \mathcal{N} \setminus \mathcal{D} && (3h)\\
\sum_{i\in\mathcal{D}} p_{d_i} &= \sum_{i\in\mathcal{D}} p_{d_i}^{\mathrm{sp}},\ p_{d_i} \ge 0 && i \in \mathcal{D} && (3i)\\
q_{d_i} &= \mu_i^{\mathrm{sp}} p_{d_i} && i \in \mathcal{N} && (3j)
\end{aligned}$$

We now explain constraints in (3). Constraint (3a) implies that the slack bus serves as an angle reference. Constraint (3b) requires that the voltage magnitude of all the PV buses and the slack bus must remain equal to the setpoint v_i^{sp} for $i \in \mathcal{V} \cup \{s\}$. Voltages of PQ buses are allowed to change as long as they remain within acceptable bounds as determined by (3c). Constraint (3d) requires that the real power generated by PQ and PV buses do not change while constraint (3e) requests that the real power of the slack bus may change within an acceptable bound. We highlight here that we implicitly assume that PV and PQ generators are not generator reserves and cannot change their real power outputs during a disturbance while the slack bus has access to a *frequency-response reserve* if needed (such an assumption is also implicitly used in [17, Eq. (1m)]) . Constraints (3f) and (3g) similarly lay out the reactive power requirements for PQ and non PQ buses, respectively.

Demand constraints are furnished by (3h)–(3j). Explicitly, for buses not participating in demand response, the real power demand must remain equal to its setpoint $p_{d_i}^{\mathrm{sp}}$. For buses participating in demand response, (3i) implies that while the

individual real power demands may vary, the total real power consumption must remain constant (this is due to frequency stability considerations, see e.g., [17]). Therefore, (3i) provides some flexibility for $i \in \mathcal{D}$. Finally, the value of reactive power demand must be such that the power factor remains constant. This requirement is dictated by constraint (3j), where $\mu_i^{\rm sp}$ is a constant that is determined by the load power factor.[1]

Consider the following non-convex optimization problem, similar to that of [17]:

$$\underset{y}{\text{minimize}} - \lambda_0(J(\theta,v)'J(\theta,v)) \text{ subject to (2) and (3),} \quad (4)$$

where the matrix J, referred to as the *power flow Jacobian*, is given below as an element of $\mathbb{R}^{(2Q+V)\times(2Q+V)}$:

$$J(\theta,v) = \begin{bmatrix} \frac{\partial \mathfrak{p}_{\mathcal{Q}\cup\mathcal{V}}}{\partial \theta_{\mathcal{Q}\cup\mathcal{V}}} & \frac{\partial \mathfrak{p}_{\mathcal{Q}\cup\mathcal{V}}}{\partial v_{\mathcal{Q}}} \\ \frac{\partial \mathfrak{q}_{\mathcal{Q}}}{\partial \theta_{\mathcal{Q}\cup\mathcal{V}}} & \frac{\partial \mathfrak{q}_{\mathcal{Q}}}{\partial v_{\mathcal{Q}}} \end{bmatrix}. \quad (5)$$

Problem (4) attempts to improve the voltage stability margin of the transmission network by maximizing the squared value of the smallest singular value (SSV) of J.

III. Solution methodology

In this Section, we propose a projected gradient-descent algorithm to approximately solve (4). The proposed algorithm features simple updates so that it can be applied to the transmission network *per-iteration* in a real-time fashion. The construction of the proposed gradient projection algorithm is similar in principle to those used in the real-time OPF literature [20]–[22]. The projection step, however, is modified for demand response to handle the simplex constraint (3i). To derive the proposed gradient projection algorithm, it is first required to introduce an alternative formulation to (4) that only depends on the real power consumption of demand-responsive loads. This is pursued in the next subsection. The description of the real-time projected gradient-descent algorithm is postponed to Section III-B.

A. Reformulation of problem (4)

Consider the operating point $y = (\theta, v, p_{\rm g}, q_{\rm g}, p_{\rm d}, q_{\rm d})$. In the context of problem (4), it turns out that the sole *controllable* quantity during demand response is $p_{{\rm d}_i}$ for $i \in \mathcal{D}$. This is explained next. The voltage angle of the slack bus, the voltage magnitude of the slack and PV buses, real power generation of PV and PQ buses, reactive power generation of PQ buses, real and reactive power demand of buses not participating in demand response (3a), (3b), (3d), (3f), (3h), and (3j). Furthermore, as dictated by constraint (3j), reactive power demand of buses participating in demand response are decided via scaling the corresponding real power demand by the constant $\mu_i^{\rm sp}$. Finally, voltages of PQ buses, real power generation of the slack bus, as well as reactive power generation of the PV buses and the slack bus are consequences of other network decisions.[2] In other words, there is no actuator "knob" that can fix these values to a desired command value. Therefore, the only remaining quantity is the real power demand of the buses participating in demand response. In essence, upon deciding the value of $p_{\mathcal{D}} := p_{{\rm d}_{\mathcal{D}}}$, the *physics* of the system automatically calculates the value of voltages of PQ buses $v_{\mathcal{Q}}$, real power generation of the slack bus $p_{{\rm g}_s}$, as well as reactive power generation of the PV buses and the slack bus $q_{{\rm g}_{\mathcal{V}\cup\{s\}}}$. This argument is formalized by using the implicit function theorem next.

Let us denote by x the uncontrollable quantities of an operating point *whilst subsuming as parameters any fixed setpoints due to constraints* (3a), (3b), (3d), (3f), (3h), *and* (3j) *and further substituting the value of* $q_{{\rm d}_i}$ *by* $\mu_i^{\rm sp} p_{{\rm d}_i}$ *for* $i \in \mathcal{D}$. We then have

$$x = (\theta_{\mathcal{Q}\cup\mathcal{V}}, v_{\mathcal{Q}}, p_{{\rm g}_s}, q_{{\rm g}_{\mathcal{V}\cup\{s\}}}). \quad (6)$$

Notice that $x \in \mathbb{R}^{2N}$ and $p_{\mathcal{D}} \in \mathbb{R}^D$ where $D < N$. Therefore, we shall interpret the power flows (2) as

$$f(x, p_{\mathcal{D}}) = 0, \quad (7)$$

where the function $f(.) : \mathbb{R}^{2N+D} \to \mathbb{R}^{2N}$ in (7) is continuously differentiable [cf. (1)]. Suppose that $\partial f/\partial x$ evaluated at the operating point $(x^0, p_{\mathcal{D}}^0)$ is invertible. Then, by the implicit function theorem [30, Theorem 9.28], x is a *locally* one-to-one function of $p_{\mathcal{D}}$ in a neighborhood $\mathcal{P}$ of $p_{\mathcal{D}}^0$, that is

$$x := x(p_{\mathcal{D}}), p_{\mathcal{D}} \in \mathcal{P} \quad (8)$$

whose Jacobian at $p_{\mathcal{D}}^0$ is computed as follows:

$$\frac{\partial x}{\partial p_{\mathcal{D}}}\Big|_{p_{\mathcal{D}}^0} = -\left(\frac{\partial f}{\partial x}\Big|_{(x^0, p_{\mathcal{D}}^0)}\right)^{-1} \frac{\partial f}{\partial p_{\mathcal{D}}}\Big|_{(x^0, p_{\mathcal{D}}^0)}. \quad (9)$$

Equation (9) is used later in this paper for computation of the gradient in our algorithm.

Leveraging (8), problem (4) is equivalent to the following problem for $p_{\mathcal{D}} \in \mathcal{P}$:

$$\begin{aligned} \underset{p_{\mathcal{D}}}{\text{minimize}} \; & -\lambda_0(J(p_{\mathcal{D}})'J(p_{\mathcal{D}})) && (10a)\\ \text{subject to (3i) and} & \\ & v_i^{\min} \le v_i(p_{\mathcal{D}}) \le v_i^{\max},\ i \in \mathcal{Q} && (10b)\\ & p_{{\rm g}_s}^{\min} \le p_{{\rm g}_s}(p_{\mathcal{D}}) \le p_{{\rm g}_s}^{\max} && (10c)\\ & q_{{\rm g}_i}^{\min} \le q_{{\rm g}_i}(p_{\mathcal{D}}) \le q_{{\rm g}_i}^{\max},\ i \in \mathcal{V}\cup\{s\}, && (10d) \end{aligned}$$

where we have slightly abused notation to denote by $J(p_{\mathcal{D}})$ the implicit dependence of $J(\theta(p_{\mathcal{D}}), v(p_{\mathcal{D}}))$ on $p_{\mathcal{D}}$ via (8). Constraints (10b)-(10d) align with the feasibility constraints encountered in a typical OPF problem. Since constraints (10b), (10c), and (10d) are not directly enforceable—as $v_{\mathcal{Q}}$, $p_{{\rm g}_s}$, and $q_{{\rm g}_{\mathcal{V}\cup\{s\}}}$ are not directly controllable by the

[1] For brevity, we have refrained from introducing in (3) the thermal loss limits for all lines $(i,j) \in \mathcal{E}$. We highlight, however, that the techniques used in this paper still carry out even if thermal limits are accounted for.

[2] Recall that in a power flow problem in transmission networks, the real and reactive power generation of the slack bus as well as the reactive power generation of PV buses are not specified and are eventually determined by the power flow solution $(\theta^*_{\mathcal{Q}\cup\mathcal{V}}, v^*_{\mathcal{Q}})$.

operator—the following penalized problem is considered [31, Section 6.2]:

$$\begin{aligned}
&\underset{p_{\mathcal{D}}}{\text{minimize}}\, \Phi(p_{\mathcal{D}};\mu) := \lambda_0 \left\{ J\left(x(p_{\mathcal{D}})\right)' J\left(x(p_{\mathcal{D}})\right) \right\} \\
&+ \sum_{i\in\mathcal{Q}} \mu_v \left\{ \phi\left(v_i(p_{\mathcal{D}}) - v_i^{\max}\right) + \phi\left(v_i^{\min} - v_i(p_{\mathcal{D}})\right) \right\} \\
&+ \mu_p \left\{ \phi\left(p_{\mathrm{g}_s}(p_{\mathcal{D}}) - p_{\mathrm{g}_s}^{\max}\right) + \phi\left(p_{\mathrm{g}_s}^{\min} - p_{\mathrm{g}_s}(p_{\mathcal{D}})\right) \right\} \\
&+ \sum_{i\in\mathcal{V}\cup\{s\}} \mu_q \left\{ \phi\left(q_{\mathrm{g}_i}(p_{\mathcal{D}}) - q_{\mathrm{g}_i}^{\max}\right) + \phi\left(q_{\mathrm{g}_i}^{\min} - q_{\mathrm{g}_i}(p_{\mathcal{D}})\right) \right\} \\
&\text{subject to (3i)}, \qquad (11)
\end{aligned}$$

where the penalty function

$$\phi(z) = \max\{z, 0\}^2 \qquad (12)$$

is used for each bound constraint along with the penalty parameters in $\mu := (\mu_v, \mu_p, \mu_q)$ for (10b), (10c), and (10d). We acknowledge here that finding an exact solution to (10) requires solving (11) for increasing values of parameter μ. However, even by a fixed moderate value of μ, numerical tests indicate satisfactory performance in maintaining the constraints.

B. Real-time projected gradient-descent

We solve problem (11) by the following projected gradient-descent algorithm:

$$p_{\mathcal{D}}^{(k+1)} = \Pi_{\mathcal{P}} \left(p_{\mathcal{D}}^{(k)} - \alpha^{(k)} \left(\frac{\partial \Phi(p_{\mathcal{D}};\mu)}{\partial p_{\mathcal{D}}} \Big|_{p_{\mathcal{D}}^{(k)}} \right)' \right) \qquad (13)$$

where $\mathcal{P}$ is the set such that (3i) is satisfied:

$$\mathcal{P} := \{ p_{\mathcal{D}} | p_{\mathcal{D}} \geq 0, \mathbf{1}' p_{\mathcal{D}} = \sum_{i\in\mathcal{D}} p_{\mathrm{d}_i}^{\mathrm{sp}} \} \qquad (14)$$

In (13), Π is the projection operator and $\alpha^{(k)}$ is a step-size parameter. Equation (13) may be equivalently reformulated as an Euclidean projection onto a probability simplex. Such a problem is solved efficiently, either by a one-dimensional bisection on the dual variable [32, Problem 1] or by a non-iterative scheme which requires sorting [33], [34].

A high-level schematic of the proposed framework is given in Fig. 1. At time step k, measurements $x(p_{\mathcal{D}}^{(k)})$ are obtained from the power network. Recall that these measurements pertain to quantities in (6), namely, voltages of PQ buses, real power of the slack bus, and reactive power of the slack and PV buses. Upon receiving the measurements $x\left(p_{\mathcal{D}}^{(k)}\right)$, the differentiation unit computes the values of the gradient $\left(\frac{\partial \Phi(p_{\mathcal{D}};\mu)}{\partial p_{\mathcal{D}}}\Big|_{p_{\mathcal{D}}^{(k)}}\right)'$, given the constant penalty parameters μ. The projection unit can then broadcast the update (13) to individual loads to encourage appropriate modification in their consumption level at iteration $k+1$.

We note that after the update $x\left(p_{\mathcal{D}}^{(k)}\right)$, the value of the objective function $\Phi(p_{\mathcal{D}}^{(k)};\mu)$ can be immediately evaluated by the objective of (11). However, the major hurdle of our approach is the computations required in the differentiation unit. Specifically, computing $\frac{\partial \Phi(p_{\mathcal{D}};\mu)}{\partial p_{\mathcal{D}}}$ is challenging. The latter computation requires knowledge of two derivatives: $\frac{\partial \lambda_0}{\partial p_{\mathcal{D}}}$ and $\frac{\partial \phi(x)}{\partial p_{\mathcal{D}}}$. For the term $\frac{\partial \lambda_0}{\partial p_{\mathcal{D}}}$, we use the known results on eigenvalue sensitivity [17]:[3]

$$\frac{\partial \lambda_0}{\partial p_{\mathrm{d}_i}} = \sum_j w_0 \frac{\partial \left(J(x)'J(x)\right)}{\partial x_j} \frac{\partial x_j(p_{\mathcal{D}})}{\partial p_{\mathrm{d}_i}} u_0, i \in \mathcal{D}. \qquad (15)$$

In (15), w_0 and u_0 are respectively the normalized left and right eigenvectors of the matrix $J(x)'J(x)$. Elements of the vector x are indexed by j. The term $\frac{\partial \left(J(x)'J(x)\right)}{\partial x_j}$ is computed by differentiating the Jacobian in (5) with respect to the element x_j. The term $\frac{\partial x_j(p_{\mathcal{D}})}{\partial p_{\mathrm{d}_i}}$ is computed using (9).

For the penalty functions, the gradient $\frac{\partial \phi(x)}{\partial p_{\mathcal{D}}}$ is computed by noting that $\frac{\partial \phi(z)}{\partial z} = 2\max\{z, 0\}$ and then using (9). Notice that the values of $\frac{\partial f}{\partial x}$ and $\frac{\partial f}{\partial p_{\mathcal{D}}}$ in (9) are simply computed by differentiating the expression in (1) correspondingly. Algorithm 1 summarizes the steps of our proposed method to maximize the SSV of the power flow Jacobian.

Algorithm 1 continues as long as the decrease at iteration k is greater than a predetermined value of ϵ. The next section numerically corroborates on several standard transmission test cases that demand response, per Algorithm 1, succeeds in improving the SSV of the power flow Jacobian.

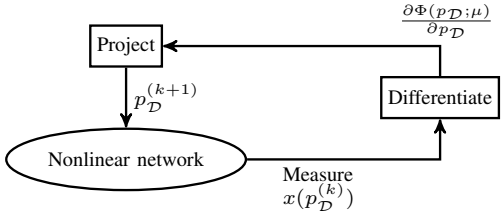

Fig. 1. A high-level schematic of the proposed framework.

Algorithm 1 Projected gradient-descent for maximizing the SSV of the power flow Jacobian

1: Select step-size parameter α, penalty parameters μ
2: Select objective improvement threshold ϵ
3: Set $\Phi(p_{\mathcal{D}}^{(-1)};\mu) = +\infty$ and $k = 0$
4: Gather measurements $x(p_{\mathcal{D}}^{(0)})$
5: Compute $\Phi(p_{\mathcal{D}}^{(0)};\mu)$ and $\frac{\partial \Phi(p_{\mathcal{D}};\mu)}{\partial p_{\mathcal{D}}}\big|_{p_{\mathcal{D}}^{(0)}}$
6: **while** $\Phi(p_{\mathcal{D}}^{(k-1)};\mu) - \Phi(p_{\mathcal{D}}^{(k)};\mu) > \epsilon$ **do**
7: Apply update (13)
8: $k \leftarrow k+1$
9: Gather measurements $x(p_{\mathcal{D}}^{(k)})$
10: Compute $\Phi(p_{\mathcal{D}}^{(k)};\mu)$ and $\frac{\partial \Phi(p_{\mathcal{D}};\mu)}{\partial p_{\mathcal{D}}}\big|_{p_{\mathcal{D}}^{(k)}}$
11: **end while**

IV. Numerical experiments

The 9-bus, 57-bus, and 118-bus transmission networks from MATPOWER [6] are considered here. Each test case is modified to contain a transmission line contingency. To this end,

[3]This derivation implicitly assumes that the considered eigenvalues of matrix $J'J$ are simple.

TABLE I
SUMMARY OF SSV IMPROVEMENT VIA REAL-TIME DEMAND RESPONSE DURING A SUSTAINED DISTURBANCE

Network	SSV before DR	SSV after DR	Improvement (%)
9-bus	0.444546	0.480698	8.13
57-bus	0.177577	0.203806	14.77
118-bus	0.153033	0.158482	3.56

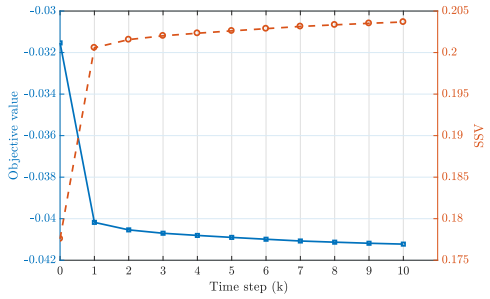

Fig. 2. Objective value and the SSV of the 57-bus network in each time step until the stopping criterion is met. Each iteration of the algorithm occurs in real-time and improves the SSV.

respectively for the 9-bus and 57-bus networks, we remove from service transmission lines $(9, 4)$ and $(11, 13)$. For the 118-bus network, transmission lines $(22, 23)$ and $(23, 24)$ are removed. Penalty parameters of $\mu_v = \mu_p = 1$ and $\mu_q = 0.1$ are chosen so that during demand response violations of reactive power limits are penalized less than those of voltage magnitude and real power. For Algorithm 1, we select a diminishing step-size of $10/\sqrt{k}$ and the stopping threshold value of $\epsilon = 0.001\Phi(p_{\mathcal{D}}^{(0)}; \mu)$.

The SSV computed for the networks with the previously-mentioned transmission line contingencies prior to and after applying the DR algorithm are respectively given in Columns 2 and 3 of Table I. Upon applying Algorithm 1, the SSV is ultimately improved. The improvement percentages are given in Column 4 of Table I. Notice that the improvement percentage is as high as 14.77% for the 57-bus network.

The evolution of the real-time Algorithm, for the 57-bus network, is shown in Figure 2. The x-axis represents time and we assume that each iteration k of the Algorithm occurs within one time unit. The left and right y-axes respectively denote the objective value $\Phi(p_{\mathcal{D}}^{(k)}; \mu)$ and the SSV at iteration k. We observe that per iteration k, the value of the objective value decreases while the SSV of the power network increases. The algorithm terminates after 10 iterations or time steps, indicating that the desired stopping criterion is met.

Changes in demand response decisions, also for the 57-bus network, are demonstrated by Fig. 3. For each bus $i \in \mathcal{D}$, the value of $p_{\mathcal{D}}^{(k)} - p_{\mathcal{D}}^{(0)}$ is plotted versus the time-step (k). For all buses participating in demand response, individual real power consumptions change over time. However, the total power demand of buses $i \in \mathcal{D}$ remains unchanged, as indicated by the blue crosses in Fig. 3.

Since our demand response program is implemented in real-time, constraint violation is inevitable. Using the penalty function (12), for the iteration set $\mathcal{K} = \{1, \ldots, k^*\}$ where k^*

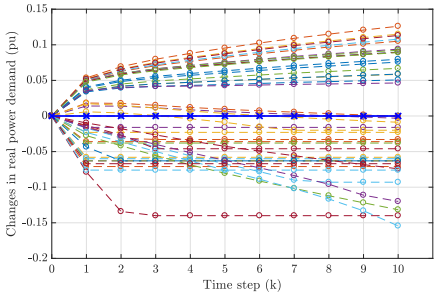

Fig. 3. Coordination of changes in real power demand from the initial pre-disturbance value. The cross markings indicate the total real power demand changes per time step. It is seen that at every time-step the total change in real power demand is zero.

TABLE II
INFEASIBILITY OF UPPER BOUND CONSTRAINTS

Network	$v_{\text{inf.}}^{\max}$ (pu)	$p_{\text{inf.}}^{\max}$ (pu)	$q_{\text{inf.}}^{\max}$ (pu)
9-bus	0.0022	0.0000	0.0000
57-bus	0.0103	0.0000	0.0379
118-bus	0.0001	0.0000	0.1417

denotes the iteration at which the stopping criterion is met, the following infeasibility indices are computed:

$$z_{\text{inf.}}^{\max} = \max_{i,k} \sqrt{\phi\left(z_i(p_{\mathcal{D}}^{(k)}) - z_i^{\max}\right)} \tag{16a}$$

$$z_{\text{inf.}}^{\min} = \max_{i,k} \sqrt{\phi\left(z_i^{\min} - z_i(p_{\mathcal{D}}^{(k)})\right)} \tag{16b}$$

In (16) the variable z and the index i represent the corresponding values outlined in constraints (10b), (10c), and (10d).

By analyzing the infeasibility indices provided in Tables II and III we find that Algorithm 1 does not significantly violate constraints (10b), (10c), and (10d). In fact, the real power provided from the slack bus always remains within its acceptable bounds at all times since $p_{\text{inf}}^{\min} = p_{\text{inf}}^{\max} = 0$ while the maximum voltage violation for the PQ buses is insignificant (below 0.0103 pu for all networks). The only major violation seems to pertain to the reactive power limits, cf. the value of 0.1417 pu for the 118-bus network. We investigate this constraint violation next.

In particular, In Fig. 4 we depict, for the 118-bus network, the upper bound violation of those generators that have, in any time step, violated their maximum limit. Immediately after the contingency at time step 0, generator 19 violates its upper reactive power limit as a consequence of network conditions. During the evolution of the algorithm, other generators gradually participate in providing reactive power and relieve the burden from generator 19. At all time steps, out of the 54 generators of the 118-bus network only 8 generators were required to increase their reactive power consumption.

V. CONCLUSION

Demand response is used in this paper to improve power system voltage stability. As the total power demand stays constant to maintain system frequency, individual buses coordinate their consumption levels to maximize the SSV of the power

TABLE III
INFEASIBILITY OF LOWER BOUND CONSTRAINTS

Network	$v_{\text{inf.}}^{\min}$ (pu)	$p_{\text{inf.}}^{\min}$ (pu)	$q_{\text{inf.}}^{\min}$ (pu)
9-bus	0.0000	0.0000	0.0000
57-bus	0.0000	0.0000	0.0000
118-bus	0.0000	0.0000	0.0446

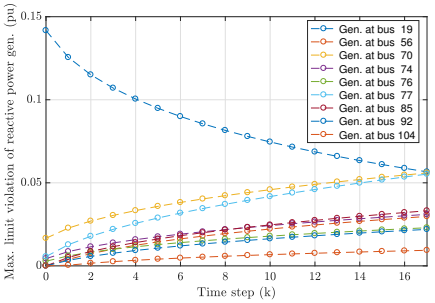

Fig. 4. Max. generator violation for the 118-bus network (only those generators that have ever violated the maximum limit are shown).

flow Jacobian as an index for voltage stability. The optimization problem is non-convex due to the power flow equations and the dependence of SSV on the operating point. The novelty of our work lies in exploiting the formulation to derive an efficient online gradient projection scheme that approximately solves the original non-convex problem. Numerical studies on sample test networks are indicative that applying our algorithm in real time leads to SSV improvement. Future work will focus on expanding the formulation to include reactive power consumption strategies for voltage stability improvement as well as comparing our methodology with traditional brute-force approaches.

REFERENCES

[1] T. V. Cutsem and C. Vournas, *Voltage stability of electric power systems*. New York: Springer, 2008.

[2] U.S.-Canada Power System Outage Task Force, "Final Report on the Blackout in the United States and Canada: Causes and Recommendations," Tech. Rep., March 2004. [Online]. Available: https://www.energy.gov/sites/prod/files/oeprod/DocumentsandMedia/BlackoutFinal-Web.pdf

[3] CIGRE Task Force 38-02-11, "Indices predicting voltage collapse including dynamic phenomena," *CIGRE publication*, 1994.

[4] V. Ajjarapu and C. Christy, "The continuation power flow: a tool for steady state voltage stability analysis," *IEEE Trans. Power Syst.*, vol. 7, no. 1, pp. 416–423, 1992.

[5] S. Greene, I. Dobson, and F. Alvarado, "Sensitivity of the loading margin to voltage collapse with respect to arbitrary parameters," *IEEE Trans. Power Syst.*, vol. 12, no. 1, pp. 262–272, 1997.

[6] R. D. Zimmerman and C. E. Murillo-Sánchez, "Matpower 6.0 User's Manual," 2016. [Online]. Available: http://www.pserc.cornell.edu/matpower/manual.pdf

[7] V. Venikov, V. Stroev, V. Idelchick, and V. Tarasov, "Estimation of electrical power system steady-state stability in load flow calculations," *IEEE Trans. Power Appar. Syst.*, vol. 94, no. 3, pp. 1034–1041, May 1975.

[8] A. Tiranuchit, L. Ewerbring, R. Duryea, R. Thomas, and F. Luk, "Towards a computationally feasible on-line voltage instability index," *IEEE Trans. Power Syst.*, vol. 3, no. 2, pp. 669–675, May 1988.

[9] P.-A. Lof, T. Smed, G. Andersson, and D. Hill, "Fast calculation of a voltage stability index," *IEEE Trans. Power Syst.*, vol. 7, no. 1, pp. 54–64, 1992.

[10] B. Cui and X. A. Sun, "A new voltage stability-constrained optimal power-flow model: Sufficient condition, socp representation, and relaxation," *IEEE Trans. Power Syst.*, vol. 33, no. 5, pp. 5092–5102, Sep. 2018.

[11] L. Aolaritei, S. Bolognani, and F. Dörfler, "A distributed voltage stability margin for power distribution networks," *IFAC-PapersOnLine*, vol. 50, no. 1, pp. 13 240 – 13 245, 2017, 20th IFAC World Congress.

[12] A. Tiranuchit and R. Thomas, "A posturing strategy against voltage instabilities in electric power systems," *IEEE Trans. Power Syst.*, vol. 3, no. 1, pp. 87–93, 2 1988.

[13] W. Rosehart, C. Canizares, and V. Quintana, "Optimal power flow incorporating voltage collapse constraints," in *Proc. IEEE Power Eng. Soc. Summer Meet. Conf. Proc.*, vol. 2, 1990, pp. 820–825.

[14] R. J. Avalos, C. A. Canizares, and M. F. Anjos, "A practical voltage-stability-constrained optimal power flow," in *Proc. IEEE Power Energy Soc. Gen. Meet. - Convers. Deliv. Electr. Energy 21st Century*, July 2008, pp. 1–6.

[15] C. Wang, B. Cui, Z. Wang, and C. Gu, "Sdp-based optimal power flow with steady-state voltage stability constraints," *IEEE Trans. Smart Grid*, vol. 10, no. 4, pp. 4637–4647, July 2019.

[16] X. Fu and X. Wang, "Determination of load shedding to provide voltage stability," *Int. J. Electr. Power Energy Syst.*, vol. 33, no. 3, pp. 515–521, Mar. 2011.

[17] M. Yao, J. L. Mathieu, and D. K. Molzahn, "Using demand response to improve power system voltage stability margins," in *Proc. IEEE Manchester PowerTech*, June 2017, pp. 1–6.

[18] M. Yao, D. K. Molzahn, and J. L. Mathieu, "The impact of load models in an algorithm for improving voltage stability via demand response," in *Proc. 55th Annu. Allert. Conf. Commun. Control. Comput.*, Oct 2017, pp. 149–156.

[19] ——, "An Optimal Power Flow Approach to Improve Power System Voltage Stability Using Demand Response," *IEEE Trans. Control. Netw. Syst.*, April 2019, to be published. [Online]. Available: https://ieeexplore.ieee.org/document/8686211

[20] L. Gan and S. H. Low, "An Online Gradient Algorithm for Optimal Power Flow on Radial Networks," *IEEE J. Sel. Areas Commun.*, no. 3, pp. 625–638, Mar. 2016.

[21] Y. Tang, K. Dvijotham, and S. Low, "Real-Time Optimal Power Flow," *IEEE Trans. Smart Grid*, vol. 8, no. 6, pp. 2963–2973, Nov. 2017.

[22] Y. Tang and S. Low, "Distributed algorithm for time-varying optimal power flow," in *Proc. 56th Annu. Conf. Decis. Control*, Dec., pp. 3264–3270.

[23] A. Bernstein and E. Dall'Anese, "Real-Time Feedback-Based Optimization of Distribution Grids: A Unified Approach," *IEEE Trans. Control. Netw. Syst.*, 2019, to be published. [Online]. Available: https://ieeexplore.ieee.org/document/8767939

[24] X. Zhou, E. Dall'Anese, L. Chen, and A. Simonetto, "An Incentive-Based Online Optimization Framework for Distribution Grids," *IEEE Trans. Autom. Control*, vol. 63, no. 7, pp. 2019–2031, 2018.

[25] K. Baker, A. Bernstein, E. Dall'Anese, and C. Zhao, "Network-cognizant voltage droop control for distribution grids," *IEEE Trans. Power Syst.*, vol. 33, no. 2, pp. 2098–2108, Mar. 2018.

[26] Y. Zhang, E. Dall'Anese, and M. Hong, "Dynamic ADMM for real-time optimal power flow," in *Proc. Glob. Conf. Signal Inf. Process.*, Nov. 2017, pp. 1085–1089.

[27] A. Hauswirth, S. Bolognani, G. Hug, and F. Dorfler, "Projected gradient descent on Riemannian manifolds with applications to online power system optimization," in *Proc. 54th Annu. Allert. Conf. Commun. Control. Comput.*, Sept. 2016, pp. 225–232.

[28] A. Hauswirth, A. Zanardi, S. Bolognani, F. Dorfler, and G. Hug, "Online optimization in closed loop on the power flow manifold," in *Proc. PowerTech Conf.*, Jun 2017, pp. 1–6.

[29] G. B. Giannakis, V. Kekatos, N. Gatsis, S.-J. Kim, H. Zhu, and B. F. Wollenberg, "Monitoring and Optimization for Power Grids: A Signal Processing Perspective," *IEEE Signal Process. Mag.*, vol. 30, no. 5, pp. 107–128, Sept. 2013.

[30] W. Rudin, *Principles of Mathematical Analysis*, 3rd ed. New York: McGraw-Hill, 1976.

[31] A. Ruszczynski, *Nonlinear Optimization*. Princeton, NJ, USA: Princeton University Press, 2006.

[32] S. Boyd, "EE364b Homework 4," Tech. Rep. [Online]. Available: https://see.stanford.edu/materials/lsocoee364b/hw4sol.pdf

[33] J. Duchi, S. Shalev-Shwartz, Y. Singer, and T. Chandra, "Efficient projections onto the l1-ball for learning in high dimensions," in *Proc. 25th Int. Conf. on Machine Learning*, ser. ICML '08. New York, NY, USA: ACM, 2008, pp. 272–279.

[34] Y. Chen and X. Ye, "Projection Onto A Simplex," Tech. Rep., 2011. [Online]. Available: http://www.math.ufl.edu/